Urea Oxidation Reaction Hot Paper

How to cite: Angew. Chem. Int. Ed. 2021, 60, 10577–10582
International Edition: doi.org/10.1002/anie.202100610
German Edition: doi.org/10.1002/ange.202100610

Regulating the Local Charge Distribution of Ni Active Sites for the Urea Oxidation Reaction

Liping Wang, Yajie Zhu, Yunzhou Wen, Shangyu Li, Chunyu Cui, Fenglou Ni, Yunxia Liu, Haiping Lin, Youyong Li, Huisheng Peng, and Bo Zhang**

Abstract: *In electrochemical energy storage and conversion systems, the anodic oxygen evolution reaction (OER) accounts for a large proportion of the energy consumption. The electrocatalytic urea oxidation reaction (UOR) is one of the promising alternatives to OER, owing to its low thermodynamic potential. However, owing to the sluggish UOR kinetics, its potential in practical use has not been unlocked. Herein, we developed a tungsten-doped nickel catalyst (Ni-WO_x) with superior activity towards UOR. The Ni-WO_x catalyst exhibited record fast reaction kinetics (440 mA cm^{-2} at 1.6 V versus reversible hydrogen electrode) and a high turnover frequency of 0.11 s^{-1}, which is 4.8 times higher than that without W dopants. In further experiments, we found that the W dopant regulated the local charge distribution of Ni atoms, leading to the formation of Ni^{3+} sites with superior activity and thus accelerating the interfacial catalytic reaction. Moreover, when we integrated Ni-WO_x into a CO_2 flow electrolyzer, the cell voltage is reduced to 2.16 V accompanying with ≈98% Faradaic efficiency towards carbon monoxide.*

Renewable-electricity-driven electrolysis systems offer great promise for sustainable energy development. For example, the electroreduction of CO_2 (CO_2R) produces value-added chemicals, including carbon monoxide (CO), formate, methane, methanol, and ethylene.[1–3] However, the energy efficiency of these electrolysis devices is greatly limited by the thermodynamically unfavorable anodic oxygen evolution half-reaction (OER).[4,5] According to a thermodynamic analysis of the overall reaction towards CO_2 electroreduction devices, 92.8% of the electricity consumption comes from OER.[6] Therefore, developing alternative anode reaction is urgently needed to radically lower energy depletion and promote its practical use.

[*] L. Wang, Y. Zhu, Y. Wen, S. Li, C. Cui, F. Ni, Prof. H. Peng, Prof. B. Zhang
State Key Laboratory of Molecular Engineering of Polymers
Department of Macromolecular Science and
Laboratory of Advanced Materials, Fudan University
Shanghai, 200438 (China)
E-mail: penghs@fudan.edu.cn
bozhang@fudan.edu.cn

Y. Liu, H. Lin, Y. Li
Institute of Functional Nano & Soft Materials (FUNSOM) and
Jiangsu Key Laboratory for Carbon-Based Functional Materials & Devices, Soochow University
Suzhou, 215123 (China)

Supporting information and the ORCID identification number for one of the authors of this article can be found under: https://doi.org/10.1002/anie.202100610.

Urea oxidation reaction (UOR) requires a thermodynamic potential of only 0.37 V, which is significantly lower than that of OER (1.23 V) and thereby would generate 70% energy saving.[7] Therefore, using thermodynamically more favorable UOR to replace the OER offers a promising and alternative strategy to improve the overall energy efficiency of electrochemical devices. Besides, UOR uses urea from industrial and sanitary wastewater (with a concentration of 0.33 M) and thus offers "cost-effective" electrons by developing renewable energy sources and sewage treatment simultaneously.

However, the intrinsically sluggish kinetics of UOR, which involves a six-electron transfer process and multiple formation/desorption of intermediates, heavily complicates the design of suitable electrocatalysts.[8] Previous studies showed that non-noble transition-metal nickel (Ni)-based compounds exhibited higher catalytic activity for UOR than other metals compounds,[7,9–11] where Ni^{3+}(NiOOH) were identified as catalytic active sites.[12] Unfortunately, these UOR catalysts still exhibit unsatisfactory activity due to the unfavorably strong absorption of the intermediate COO* on Ni^{3+} sites.[13] It is reported that the adsorption energy of intermediates was closely related to its electronic structures.[14–17] Thus, regulating the electronic structures of Ni^{3+} sites may construct catalytic sites with high UOR intrinsic activity.

It is known that high-valence chromium (Cr), molybdenum (Mo), tungsten (W) and vanadium (V) have great capability of modulating the electronic structures in other catalysis systems.[18–22] By virtue of structurally versatile coordination property,[23] we focus in particular on W to regulate the electronic structure of Ni site, expecting to weaken the adsorption of COO* intermediate on catalytic sites.[24]

Herein, we successfully prepared the Ni-based catalyst with homogeneous W dopant, which exhibited a record high current density of 440 mA cm^{-2} at 1.6 V versus reversible hydrogen electrode (RHE) in 1 M KOH with 0.33 M urea, remarkably outperforming the state-of-art UOR catalyst. The in situ synchrotron-based X-ray absorption near-edge structure (XANES) reveals that the enhanced performance is attributed to the transfer of outer-layer electron from Ni atoms to adjacent W atoms. Finally, we coupled UOR with the cathodic CO_2R in a CO_2 electrolyzer, which lowered the cell voltage by 370 mV compared to OER. The designed UOR//CO_2R system is expected to be a promoter of high-efficiency energy-related and sewage-treatment system towards carbon-neutral goal.

 © 2021 Wiley-VCH GmbH

The Ni-W binary pre-catalyst was synthesized via a simple two-step method (Figure 1a and Supplementary Information (SI)), a facile coprecipitation process and followed with annealing under hydrogen/argon (550 °C, H_2:Ar = 5:95) atmosphere (Note S2). After electrochemically activated at the potential of 1.1 V–1.6 V in 1 M KOH, the electrocatalyst was obtained and denoted as Ni-WO_x. The control samples with different W:Ni ratios were prepared via the same method (Figure S1). The scanning electron microscopy (SEM) image showed a sphere-like morphology with an average size of 100 nm (Figure 1b). The high-resolution transmission electron microscopy (HRTEM) (Figure 1c) revealed an expanded lattice spacing of 0.214 nm in Ni-WO_x sample, which was larger than NiO (200) plane (0.209 nm). This lattice spacing deviation indicated that W was introduced into the lattice of NiO and enlarged the original lattice spacing, as reported in other materials.[25,26] The elemental mapping obtained by energy dispersive X-ray spectroscopy (EDS) confirmed the homogeneous distribution of Ni, W and O (Figure 1d–g) with a Ni/W molar ratio of 3.13 (Figure S2), consistent with the results of inductively coupled plasma-mass spectrometry (ICP-MS) measurements (Table S1). The X-ray diffraction (XRD) patterns and HRTEM together indicated that the Ni-WO_x catalyst was composed of surface W-doped Ni oxides and bulk W-doped metallic Ni (Figure S3). Overall, these results proved that the W atoms were successfully incorporated into Ni lattice with a uniform distribution.

We next tested the UOR catalytic performance of a series of Ni-WO_x, in a standard three-electrode electrochemical cell (Figure S4). The OER and UOR activity of the best performed Ni-WO_x was evaluated by linear sweep voltammetry (LSV) in 1 M KOH and 1 M KOH with 0.33 M urea, respectively. As can be seen in Figure 2a, Ni-WO_x required a potential of 1.40 V to drive a current density of 100 mA cm^{-2} when catalyzing UOR, negatively shifted by 273 mV compared to that of OER. This result indicated that UOR was more conducive to occur at low potential than OER (Figure 2a, inset). As shown in Figure 2b, the potential of Ni-WO_x required to reach 100 mA cm^{-2} for UOR is 80 mV lower than that of NiO_x, indicating that the Ni sites regulated by W appreciably possess high catalytic activity for UOR. The WO_2 and bare Ni foam displayed low current density, demonstrating that W sites and the substrate contributed negligible activities during UOR. Moreover, the Ni-WO_x catalyst showed an obviously higher current density at 1.6 V (440 mA cm^{-2}) than NiO_x catalyst (182 mA cm^{-2}), manifesting its faster reaction kinetics.

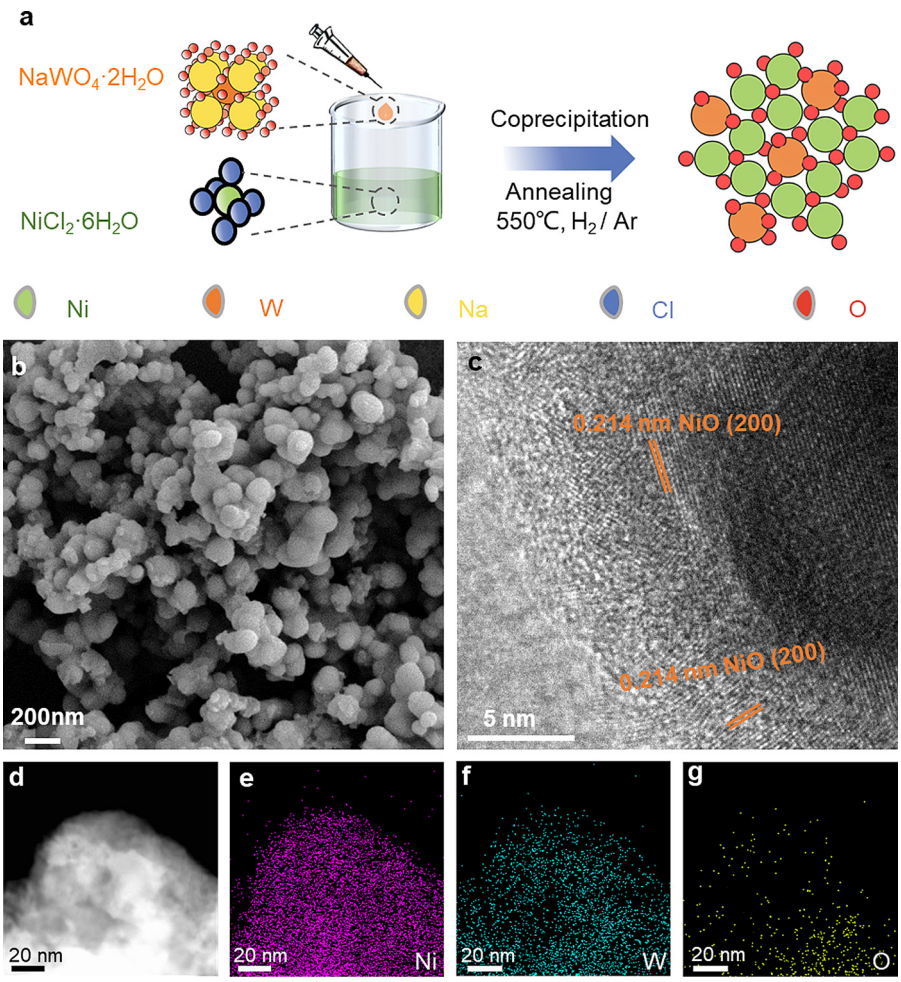

Figure 1. Synthesis and characterization of Ni-WO_x. a) Schematic illustration of the synthesis of the Ni-WO_x catalyst. b) SEM image of Ni-WO_x. c) HRTEM images of Ni-WO_x and the corresponding lattice spacings. d–g) HRTEM image and corresponding EDS results of Ni-WO_x: Ni (purple), W (blue), and O (yellow).

The UOR kinetics of different catalysts was further investigated by corresponding Tafel plots and electrochemical impedance spectroscopy (EIS). As shown in Figure 2c, the Tafel slope of Ni-WO_x was calculated as about 39 mV dec^{-1}, which is much lower than that of NiO_x (191 mV dec^{-1}), confirming the faster reaction kinetics of Ni-WO_x. The significant difference of Tafel slopes of the two catalysts is possibly due to the different rate-determining steps (RDS). According to our previous research,[13] the RDS of Ni-WO_x is the -CNO desorption step because of the regulation effect of W, while the RDS of NiO_x is the CO_2 desorption step (Table S3). The charge transfer resistance (R_{ct}) obtained from EIS is also related to the UOR kinetics at Ni-WO_x/electrolyte interface (Figure S6). The R_{ct} values for Ni-WO_x is 6.2 Ω, which is obviously smaller than that of NiO_x (812 Ω), revealing that Ni-WO_x possessed a faster UOR rate than NiO_x, which is in line with the Tafel slope results.

To evaluate the intrinsic activity of these catalysts, we calculated the turnover frequency (TOF) according to the total catalyst loading mass

 © 2021 Wiley-VCH GmbH

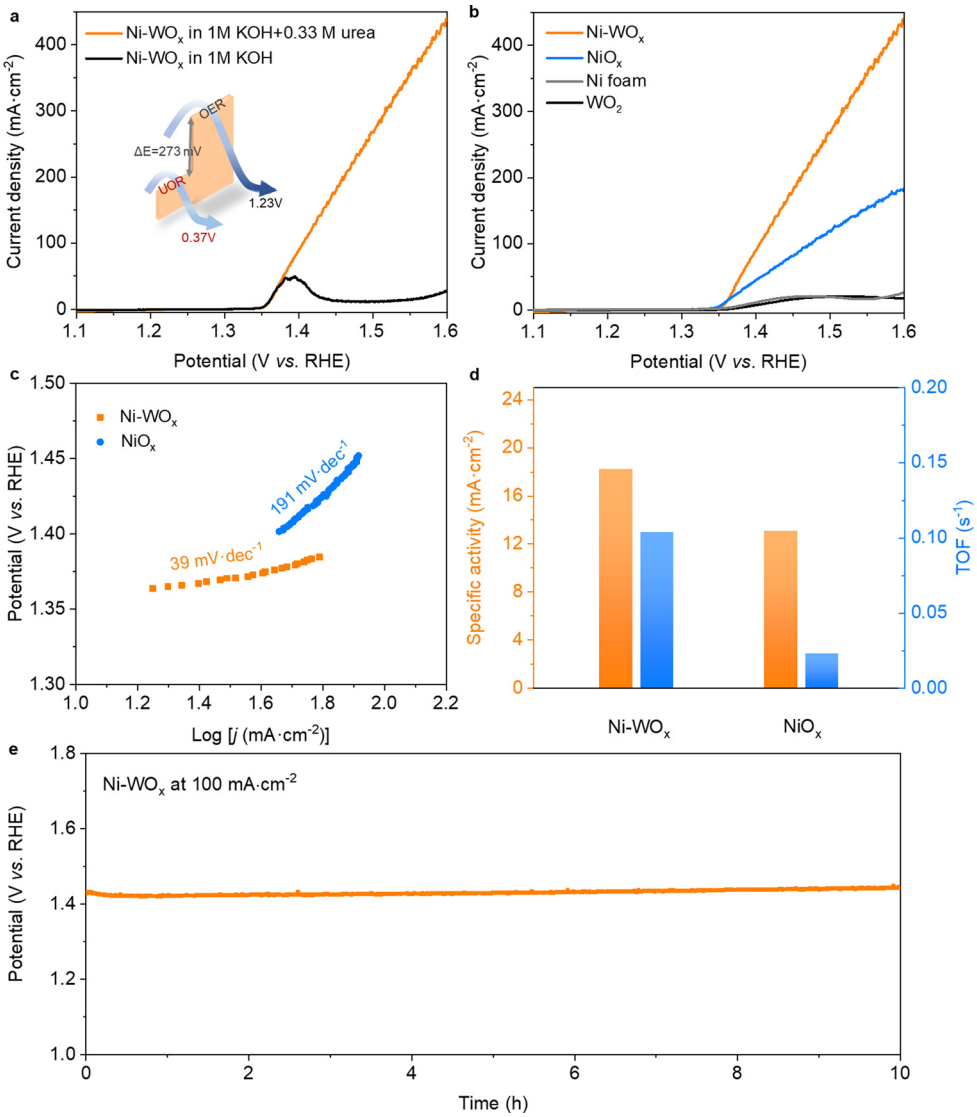

Figure 2. Electrocatalytic UOR performance. a) Polarization curves of Ni-WO$_x$ in 1 M KOH with and without 0.33 M urea at a scan rate of 10 mV s^{-1}; the inset shows an energy diagram representing the kinetics of OER and UOR. b) UOR polarization curves of Ni-WO$_x$, NiO$_x$, WO$_2$, and Ni foam as bare substrates. c) Tafel plots and d) the specific activities (ECSA-normalized current density, left) and TOF plots (calculated by total Ni atoms, right) of Ni-WO$_x$ and NiO$_x$, respectively. e) Chronoamperometric curves at a constant current density of 100 mA cm^{-2} for Ni-WO$_x$ in 1 M KOH with 0.33 M urea.

(Note S8). As can be seen from Figure 2d, the TOF of Ni-WO$_x$ (0.11 s^{-1}) showed 4.8 times higher intrinsic activity than that of NiO$_x$ (0.023 s^{-1}). Furthermore, we normalized the current density using the electrochemically active surface areas (ECSA), which obtained from electrochemical double-layer capacitance (C_{dl}) measurements (Figure S7), loading-mass and BET area (Figure S8). The specific activities (ECSA-normalized current density), mass activities (loading-mass-normalized current density) and BET normalized activities of Ni-WO$_x$ catalyst are 1.4, 2.4 and 1.1 times higher than those of NiO$_x$ at 1.6 V (Figure 2d, Figure S9 and Table S4), indicating that Ni-WO$_x$ exhibited higher intrinsic activity than NiO$_x$. Besides, stability is also a crucial parameter to evaluate the long-term UOR catalytic activity of the electrocatalysts. The chronoamperometric response test was conducted at a constant current density of 100 mA cm^{-2}, and a stable voltage of about 1.42 V was sustained for 10 h with negligible degradation.

To gain more insights into the influence of W incorporation on Ni at atomic level during the UOR catalyst process, we carried out in situ X-ray adsorption spectroscopy (XAS) and X-ray photoelectron spectroscopy (XPS) to probe the electronic and coordination structures of Ni-WO$_x$ and NiO$_x$. In W L$_3$-edge X-ray adsorption near-edge structure (XANES) of Ni-WO$_x$ at different potentials (Figure 3a), the absorption threshold showed a shift to lower energy at 1.6 V, indicating an increase of *d*-band occupy states on W atoms.[27] Furthermore, white-line position of W in Ni-WO$_x$ sample as a function of the formal *d*-band hole numbers (Figure 3b) significantly illustrated that the number of electrons on the *d* orbital increased after applying the potential, which may be attributed to the electron transfer from adjacent Ni atoms to W atoms. The local structure and coordinating situation around W were determined by Fourier transform (FT) of extended X-ray absorption fine structure (EXAFS) spectra (Figure 3c). Only the Ni-W scatterings were observed at ≈2.52 Å, suggesting that all the W atoms were surrounded by Ni neighbors.[21,28] In addition, the intensity of Ni-W peak showed an enhancement for Ni-WO$_x$ under the applied potential, demonstrating a stronger Ni-W correlations and corresponding coordination geometry. Strikingly, both the intensity of the W-O peak and fitted W-O coordination number (Figure S10 and Table S5) of Ni-WO$_x$ at 1.6 V (1.87 Å) are lower than that of pristine Ni-WO$_x$ (2.00 Å), suggesting the presence of oxygen vacancies in bulk. Moreover, in XPS O 1s spectra, the observed signal can be divided into three peaks. The peak located at around 530.5 and 532.7 eV can be ascribed to the lattice oxygen and the absorbed H_2O on the catalyst surface, respectively. The peak located at around 531.4 eV can be attributed to oxygen vacancies (Figure S11), which brings synergetic effects of

 © 2021 Wiley-VCH GmbH

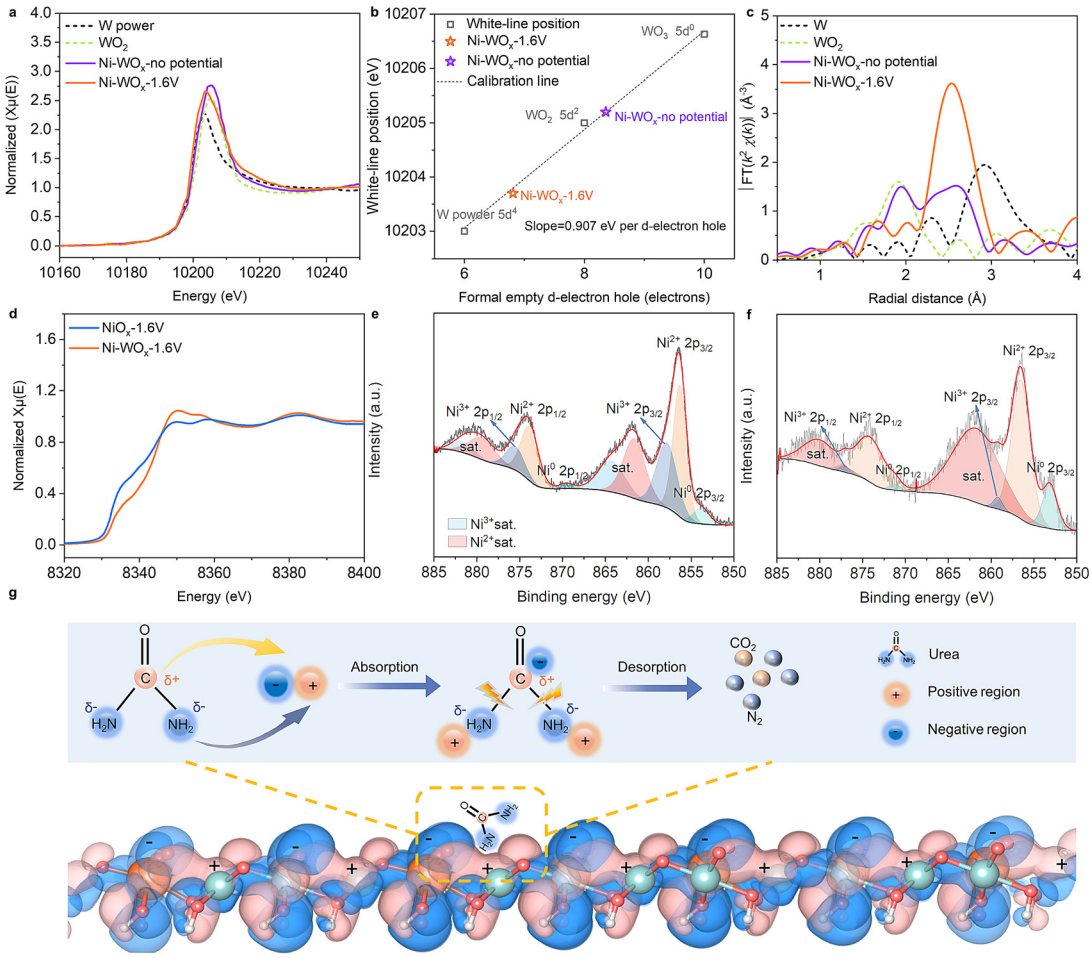

Figure 3. Electronic structure analyses of Ni-WO_x and NiO_x. a) W L_3-edge XANES spectra for Ni-WO_x. b) White-line position of Ni-WO_x (pentastar) as a function of the formal *d*-band hole numbers. Formal *d*-band hole values were calculated based on the white-line shift and the increase of 0.907 eV per *d*-band hole calibrated from W powder ($5d^4$), WO_2 ($5d^2$), and WO_3 ($5d^0$) standards. c) The W L_3-edge Fourier transforms of k^2-weight EXAFS spectra for Ni-WO_x. d) Ni K-edge XANES spectra for Ni-WO_x–1.6 V and NiO_x–1.6 V, respectively. e,f) High-resolution Ni 2p XPS spectra of Ni-WO_x and NiO_x after reaction, respectively. g) Charge density difference for Ni-WO_x from DFT calculations.

faster electron transport and enhancement of catalytic activity of UOR catalysts.[11]

The normalized Ni K-edge XANES spectra of Ni-WO_x and NiO_x under the applied potential of 1.6 V were shown in Figure 3d. The adsorption edge of Ni-WO_x is positively shifted towards higher energy than that of NiO_x, indicating that Ni is more likely to be oxidized after introducing W. In comparison with NiO_x (2.48 Å), the peak position of Ni-Ni scattering for Ni-WO_x (2.52 Å) had an appreciably right shift (Figure S12). The fitting results of Ni K-edge showed that both the Ni-Ni bonds and Ni-W bonds were contained in Ni K-edge EXAFS spectrum (Figure S13 and Table S6), which was consistent with the W L_3-edge EXAFS results. The incorporation of W into Ni lattice, make a change of the chemical environment of Ni and W.

To gain more investigation on the formation of Ni^{3+} active sites on catalyst surface after W incorporation, we further carried out XPS measurements of Ni-WO_x and NiO_x samples. In the high-resolution Ni 2p spectra (Figure 3e and f), the binding energy of Ni $2p_{3/2}$ and Ni $2p_{1/2}$ can be deconvoluted into two peaks. The peak centered at 856.3 and 873.9 eV can be ascribed to Ni^{2+}, while the peaks located at 857.8 eV and 875.5 eV can be attributed to Ni^{3+},[26,29,30] which originate from the oxidation of Ni in Ni-WO_x compounds. It is noteworthy that the percentage of Ni^{3+} on the surface of Ni-WO_x are higher compared to NiO_x, suggesting that more Ni^{3+} active sites are formed in the Ni-WO_x catalyst than in NiO_x. That means, the electrons of Ni are prone to transfer to W then increased the valence state of Ni, demonstrating that W modifies the electronic structures of Ni sites. These results, taken together, reveal that the superior electrocatalytic activity of Ni-WO_x is due to the optimal charge distribution amongst W and Ni sites, where W atoms can attract electrons from adjacent Ni atoms and facilitate the formation of Ni^{3+} active sites, thus accelerating UOR.

To understand the benefit of the charge-transfer interaction between W and Ni atoms in accelerating UOR process, we carried out computational studies for the charge difference between W and Ni atoms (Figure 3g). In our calculations, W-doped NiOOH was considered as the catalyst

 © 2021 Wiley-VCH GmbH

model (Figure S14 and Note S9) which was based on the removal of the surface hydrogen on Ni-$(OH)_2$. Because the surface hydrogen is unstable in electrochemical reaction.[31,32] Therefore, the surface hydrogen atoms are removed to mimic the realistic catalyst. As a result, the transition metal atoms are exposed and serve as active sites for UOR. The calculated charge difference between W doped and undoped catalysts reveals that W doping results in an electron transfer from Ni to W, indicating that the oxidation states of Ni atoms increased. When UOR occurs on the surface of Ni-WO_x catalyst, the "electron-withdrawing" group of carbonyl (C=O) will be intensively absorbed on the negative region, whereas the "electron-donating" group of amino ($-NH_2$) is prone to absorbed on the positive region, facilitating the decomposition of urea molecules. Therefore, the charge distribution surface regulated by W resulted in high UOR activities and accelerated UOR kinetics.

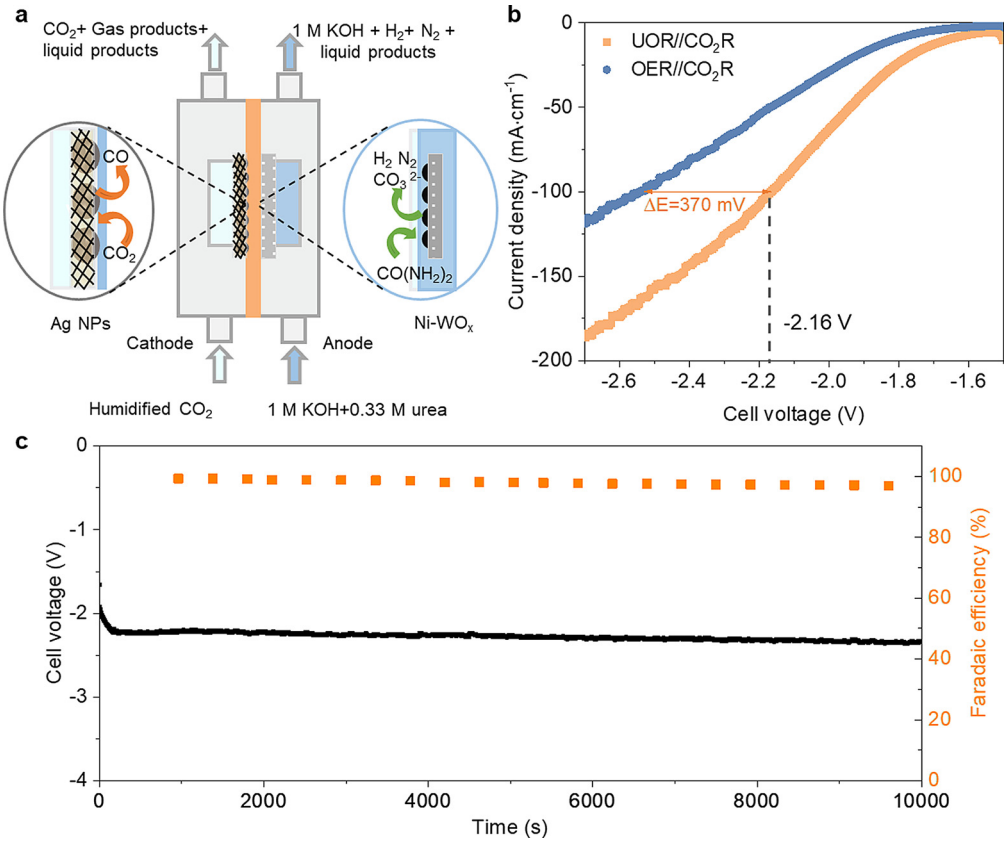

Figure 4. Demonstration of UOR combined with CO_2R. a) The schematic image of the UOR//CO_2R electrolyzer. b) Polarization curves of the electrolyzer in 1 M KOH with and without 0.33 M urea at scan rate of 10 mV s^{-1}. c) Cell voltage as a function of time recorded with the anodic Ni-WO_x electrode and cathodic Ag NPs electrode at a current density of 100 mA cm^{-2} and the corresponding Faradaic efficiency from the chromatographic measurement of evolved CO.

To verify the feasibility of UOR as an alternative anodic reaction, we made a thermodynamic analysis (Table S7 and Note S10) and assembled a flow electrolyzer. The cell used Ni-WO_x as anodic electrocatalyst for UOR and commercial Ag nanoparticles (Ag NPs) as cathodic catalyst for CO_2 electroreduction (Note S11). The design of the electrolyzer is schematically illustrated in Figure 4a. For comparison, 1 M KOH with and without 0.33 M urea were chosen as electrolytes. The benefit of UOR in lowering cell potential was verified by the polarization curves (Figure 4b). The electro-oxidation of urea coupled to electroreduction of CO_2 resulted in a significantly decrease of the cell voltage (2.16 V) to drive a current density of 100 mA cm^{-2} for CO formation and urea decomposition, which is 370 mV lower than the system using OER as anodic reaction, saving 15% energy (Note 11). To ensure the cathodic CO_2 electroreduction remains unaffected by the urea in electrolyte, a durability plot of the electrolyzer was carried out and the result was shown in Figure 4c. Cathodic CO_2 electroreduction produced CO at a Faradaic efficiency of 98%, the corresponding gas production analysis was shown in Figure S15a. Moreover, there was no signal at chemical shift of formate (8.34 ppm) and urea (5.60 ppm), according to the NMR spectra (Figure S15b and Figure S15c), indicating the high selectivity of the CO product and good performance of urea decomposition.

In summary, this work described how the incorporation of high-valence W promote the catalytic activity of Ni active sites for UOR. We offer a modulating strategy enabling the partial electrons transfer from Ni to W to create electrocatalytic active sites with high intrinsic activity. Besides, by replacing conventional anodic half-reaction OER with UOR, we achieved a low cell potential of 2.16 V in a CO_2-to-CO electrolyzer and saved 15% energy compared to traditional OER, showing a promising future of the industrialization of CO_2 electroreduction and other energy-related technologies.

Acknowledgements

This work was supported by NSFC (21875042, 21634003, 51573027), MOST (2016YFA0203302), and STCSM (18QA140080, 16JC1400702). This work was also supported by the Program for Eastern Scholars at Shanghai Institutions.

 © 2021 Wiley-VCH GmbH

Conflict of interest

The authors declare no conflict of interest.

Keywords: electrocatalysis · energy conversion · nickel · urea oxidation reaction

[1] F. P. García de Arquer, C. T. Dinh, A. Ozden, J. Wicks, C. McCallum, A. R. Kirmani, D. H. Nam, C. Gabardo, A. Seifitokaldani, X. Wang, Y. C. Li, F. Li, J. Edwards, L. J. Richter, S. J. Thorpe, D. Sinton, E. H. Sargent, *Science* **2020**, *367*, 661–666.
[2] W. Ma, S. Xie, T. Liu, Q. Fan, J. Ye, F. Sun, Z. Jiang, Q. Zhang, J. Cheng, Y. Wang, *Nat. Catal.* **2020**, *3*, 478–487.
[3] M. Liu, Y. Pang, B. Zhang, P. De Luna, O. Voznyy, J. Xu, X. Zheng, C. T. Dinh, F. Fan, C. Cao, F. P. de Arquer, T. S. Safaei, A. Mepham, A. Klinkova, E. Kumacheva, T. Filleter, D. Sinton, S. O. Kelley, E. H. Sargent, *Nature* **2016**, *537*, 382–386.
[4] S. Chu, A. Majumdar, *Nature* **2012**, *488*, 294–303.
[5] D. Y. C. Leung, G. Caramanna, M. M. Maroto-Valer, *Renewable Sustainable Energy Rev.* **2014**, *39*, 426–443.
[6] S. Verma, S. Lu, P. J. A. Kenis, *Nat. Energy* **2019**, *4*, 466–474.
[7] B. K. Boggs, R. L. King, G. G. Botte, *Chem. Commun.* **2009**, 4859–4861.
[8] R. P. Forslund, C. T. Alexander, A. M. Abakumov, K. P. Johnston, K. J. Stevenson, *ACS Catal.* **2019**, *9*, 2664–2673.
[9] D. Zhu, C. Guo, J. Liu, L. Wang, Y. Du, S. Z. Qiao, *Chem. Commun.* **2017**, *53*, 10906–10909.
[10] J. Xie, W. Liu, F. Lei, X. Zhang, H. Qu, L. Gao, P. Hao, B. Tang, Y. Xie, *Chem. Eur. J.* **2018**, *24*, 18408–18412.
[11] Y. Tong, P. Chen, M. Zhang, T. Zhou, L. Zhang, W. Chu, C. Wu, Y. Xie, *ACS Catal.* **2018**, *8*, 1–7.
[12] D. A. Daramola, D. Singh, G. G. Botte, *J. Phys. Chem. A* **2010**, *114*, 11513–11521.
[13] L. Zhang, L. Wang, H. Lin, Y. Liu, J. Ye, Y. Wen, A. Chen, L. Wang, F. Ni, Z. Zhou, S. Sun, Y. Li, B. Zhang, H. Peng, *Angew. Chem. Int. Ed.* **2019**, *58*, 16820–16825; *Angew. Chem.* **2019**, *131*, 16976–16981.
[14] Z. W. Seh, J. Kibsgaard, C. F. Dickens, I. Chorkendorff, J. K. Norskov, T. F. Jaramillo, *Science* **2017**, *355*, eaad4998.
[15] D. Voiry, R. Fullon, J. Yang, E. S. C. de Carvalho Castro, R. Kappera, I. Bozkurt, D. Kaplan, M. J. Lagos, P. E. Batson, G. Gupta, A. D. Mohite, L. Dong, D. Er, V. B. Shenoy, T. Asefa, M. Chhowalla, *Nat. Mater.* **2016**, *15*, 1003–1009.
[16] L. Zhang, H. Yuan, L. Wang, H. Zhang, Y. Zang, Y. Tian, Y. Wen, F. Ni, H. Song, H. Wang, B. Zhang, H. Peng, *Sci. China Mater.* **2020**, *63*, 2509–2516.
[17] C. C. Li, Y. W. Liu, Z. W. Zhuo, H. X. Ju, D. Li, Y. P. Guo, X. J. Wu, H. Q. Li, T. Y. Zhai, *Adv. Energy Mater.* **2018**, *8*, 1801775.
[18] L. Wang, M. Li, Z. Huang, Y. Li, S. Qi, C. Yi, B. Yang, *J. Power Sources* **2014**, *264*, 282–289.
[19] Z. L. Wang, W. J. Liu, Y. M. Hu, M. L. Guan, L. Xu, H. P. Li, J. Bao, H. M. Li, *Appl. Catal. B* **2020**, *272*, 118959.
[20] Z. Chen, Y. Song, J. Cai, X. Zheng, D. Han, Y. Wu, Y. Zang, S. Niu, Y. Liu, J. Zhu, X. Liu, G. Wang, *Angew. Chem. Int. Ed.* **2018**, *57*, 5076–5080; *Angew. Chem.* **2018**, *130*, 5170–5174.
[21] Y. Duan, Z. Y. Yu, L. Yang, L. R. Zheng, C. T. Zhang, X. T. Yang, F. Y. Gao, X. L. Zhang, X. Yu, R. Liu, H. H. Ding, C. Gu, X. S. Zheng, L. Shi, J. Jiang, J. F. Zhu, M. R. Gao, S. H. Yu, *Nat. Commun.* **2020**, *11*, 4789.
[22] J. Yan, L. Kong, Y. Ji, J. White, Y. Li, J. Zhang, P. An, S. Liu, S. T. Lee, T. Ma, *Nat. Commun.* **2019**, *10*, 2149.
[23] B. Zhang, X. Zheng, O. Voznyy, R. Comin, M. Bajdich, M. Garcia-Melchor, L. Han, J. Xu, M. Liu, L. Zheng, F. P. Garcia de Arquer, C. T. Dinh, F. Fan, M. Yuan, E. Yassitepe, N. Chen, T. Regier, P. Liu, Y. Li, P. De Luna, A. Janmohamed, H. L. Xin, H. Yang, A. Vojvodic, E. H. Sargent, *Science* **2016**, *352*, 333–337.
[24] S. Lu, J. Pan, A. Huang, L. Zhuang, J. Lu, *Proc. Natl. Acad. Sci. USA* **2008**, *105*, 20611–20614.
[25] S. Deng, F. Yang, Q. Zhang, Y. Zhong, Y. Zeng, S. Lin, X. Wang, X. Lu, C. Z. Wang, L. Gu, X. Xia, J. Tu, *Adv. Mater.* **2018**, *30*, 1802223.
[26] Z. Ji, J. Liu, Y. Deng, S. Zhang, Z. Zhang, P. Du, Y. Zhao, X. Lu, *J. Mater. Chem. A* **2020**, *8*, 14680–14689.
[27] H. N. Nong, T. Reier, H.-S. Oh, M. Gliech, P. Paciok, T. H. T. Vu, D. Teschner, M. Heggen, V. Petkov, R. Schlögl, T. Jones, P. Strasser, *Nat. Catal.* **2018**, *1*, 841–851.
[28] X. Zhang, S. Han, B. Zhu, G. Zhang, X. Li, Y. Gao, Z. Wu, B. Yang, Y. Liu, W. Baaziz, O. Ersen, M. Gu, J. T. Miller, W. Liu, *Nat. Catal.* **2020**, *3*, 411–417.
[29] V. R. Jothi, K. Karuppasamy, T. Maiyalagan, H. Rajan, C. Y. Jung, S. C. Yi, *Adv. Energy Mater.* **2020**, *10*, 1904020.
[30] R. Ding, L. Qi, M. Jia, H. Wang, *Nanoscale* **2014**, *6*, 1369–1376.
[31] D. H. Napper, *J. Colloid Interface Sci.* **1970**, *33*, 384–392.
[32] D. Yang, Z. Su, Y. Chen, K. Srinivas, J. Gao, W. Zhang, Z. Wang, H. Lin, *Small* **2020**, *16*, 2006881.

Manuscript received: January 14, 2021
Accepted manuscript online: February 25, 2021
Version of record online: March 30, 2021

 © 2021 Wiley-VCH GmbH